ARTICLES

Deuteron breakup reaction ^{2}H($\vec{p}$,pp)n induced by polarized protons at E_p=19.0 MeV

H. Patberg, R. Großmann, G. Nitzsche, L. Sydow, S. Vohl, and H. Paetz gen. Schieck
Institut für Kernphysik, Universität zu Köln, D-50937 Köln, Germany

J. Golak and H. Witała
Institute of Physics, Jagellonian University, PL-30059 Cracow, Poland

W. Glöckle and D. Hüber
Institut für Theoretische Physik II, Ruhr-Universität Bochum, D-44780 Bochum, Germany

(Received 27 November 1995)

We measured cross sections and vector analyzing powers of the breakup reaction ^{2}H($\vec{p}$,pp)n at a laboratory proton energy of 19.0 MeV in four kinematically complete arrangements comprising space star, collinearity, final-state interaction, and quasifree scattering conditions. We present our results and compare them to the predictions of rigorous three-nucleon Faddeev calculations using different realistic nucleon-nucleon potentials. We found cases of good agreement but also cases of clear discrepancies. The inclusion of the 2π-exchange Tucson-Melbourne three-nucleon force does not remove these discrepancies but even worsens the description in all cases. In the quasifree scattering and space star configurations Coulomb-force effects might possibly be responsible for at least part of the observed discrepancies.

PACS number(s): 21.45.+v, 21.30.Fe, 24.70.+s, 25.10.+s

I. INTRODUCTION

Only since the advent of rigorous solutions for the three-nucleon ($3N$) Faddeev equations in the scattering domain [1,2] a quantitatively meaningful comparison of theoretical predictions and $3N$ data can be performed. Since these calculations are based on realistic nucleon-nucleon (NN) potentials the $3N$ system has thus become an important testing ground for modern NN interactions. Furthermore, new features, absent in $2N$ systems, such as off-shell effects and three-body forces may appear in the $3N$ system.

Despite recent progress in this field the situation is far from satisfactory and many questions are left unanswered. The comparison of $3N$ breakup data with the results of recent rigorous Faddeev calculations shows that there are cases of quantitative agreement [3–6], but also examples of clear discrepancies [3,5,7,8]. In the case of kinematically complete breakup cross sections one finds regions in the phase space of three outgoing nucleons where the theory cannot reproduce the absolute magnitude of the cross sections [5,7,8]. This is true both for neutron-deuteron (nd) [7] as well as for proton-deuteron (pd) data [5,8] which may be additionally influenced by Coulomb-force effects. In the case of breakup vector analyzing powers the situation is somewhat unclear because of the poorer database. Recent A_y data from a pd breakup measurement at 65 MeV [6,9,10] show generally good agreement with theoretical predictions based on realistic NN interactions. At low energies, where a clear-cut discrepancy between theory and data has been found for the elastic scattering vector analyzing power A_y [3,11], breakup vector analyzing power data are rare.

In this paper we present new experimental data for the cross section and vector analyzing power in the proton induced deuteron breakup $p_1+d_2\rightarrow p_3+p_4+n_5$. We investigate this process using polarized protons of 19 MeV laboratory energy. The differential cross sections $d^3\sigma/d\Omega_3 d\Omega_4 dS$ and the vector analyzing powers $A_y(S)$, parametrized by the arc length S of the kinematical curve, are measured in four kinematically complete configurations comprising ''classical'' geometries: np final-state interaction (FSI) (equal momenta of the neutron and proton), pp asymmetric collinearity (COL) (the undetected neutron is at rest in the center-of-mass system), space star (SST) (in the center-of-mass system all momenta of the outgoing nucleons lie in the same plane which is perpendicular to the beam direction and form an equilateral triangle), and pp quasifree scattering (QFS) (the undetected neutron is at rest in the laboratory system).

In Sec. II we give a brief sketch of the theoretical formalism. Section III describes the experimental setup and in Sec. IV the details of our method of data analysis are outlined. The comparison of data to theory and the discussion of the results follow in Sec. V and a summary is given in Sec. VI.

II. THEORY

The theoretical results presented in this paper are based on rigorous solutions of the $3N$ Faddeev equations using different realistic NN interactions. In the following we give a short presentation of our formalism and numerical performance.

When only NN interactions are active and neglecting the long-range Coulomb force we solve the Faddeev equation for the T operator

$$T = tP + tPG_0T, \tag{2.1}$$

where G_0 is the free three-body propagator and t is the two-body off-shell t matrix. P denotes a sum of cyclic and anticyclic permutations of three nucleons. After solving Eq. (2.1) the breakup-transition operator U_0 follows by quadrature:

$$U_0 = (1+P)T. \tag{2.2}$$

In the case when the potential energy of the $3N$ system contains in addition to the pure NN interaction also a term coming from a three-nucleon force (3NF), we introduce the operator $t_4 = V_4 + V_4G_0t_4$, driven by the three-nucleon interaction V_4. Now in the transition operator U_0 a new term T_4 on top of the T appears. Both T and T_4 fulfill the following set of coupled equations:

$$T = tP + tG_0T_4 + tPG_0T, \tag{2.3}$$

$$T_4 = (1+P)t_4 + (1+P)t_4G_0T. \tag{2.4}$$

These equations are solved in a perturbative approach in powers of V_4 and the different orders are then summed up by the Padé method. The breakup amplitude is then given by

$$U_0 = (1+P)T + T_4. \tag{2.5}$$

The physical content of Eqs. (2.1), (2.3), and (2.4) is revealed after iterating them. The resulting multiple scattering series describes contributions from scattering processes where three nucleons interact with two- or three-body forces with free propagation in between. For more details of the theoretical formulation and numerical performance we refer to [1,2,12] and references therein.

We solved Eq. (2.1) using the following realistic NN potentials: AV14 [14], Bonn-B [15], Nijmegen78 [16], and Paris [17]. In all cases the charge-independence breaking (CIB) of the NN interaction in the state $^1S_0$ was treated exactly by including an admixture of total isospin $T=\frac{3}{2}$ [13]. Such CIB requires different $^1S_0$ NN interactions in the two-body subsystems (pp and np) of the pd system. This was achieved by applying the $^1S_0$ np interaction of the Bonn-B potential in the Nijmegen78 and Paris potential calculations and the $^1S_0$ pp interaction of a $^1S_0$ pp modified version of the Bonn-B potential [15] in the AV14 and Bonn-B potential calculations.

Such an artificial mixing of different $^1S_0$ forces can now be avoided with the appearance of recently updated high quality NN interactions: AV18 [18], CD Bonn [19], and Nijmegen 93, I and II [20]. All these interactions are charge dependent in isospin $t=1$ states having thus inherently built-in differences in the $^1S_0$ force component for np, pp, and nn systems. Contrary to the previously mentioned older potentials they are practically on-shell equivalent and describe the $2N$ data with impressively good quality characterized by $\chi^2 \approx 1$ per degree of freedom. We also solved Eq. (2.1) using all these new interactions.

In order to gain some insight into possible 3NF effects we included also the Tucson-Melbourne (TM) three-nucleon force [21,22] in our Bonn-B calculation. From our previous study we know that effects of this 3NF depend strongly on the value of the cut-off parameter Λ_π appearing in the πNN form factor. In the present calculations we use the "recommended" value for this parameter $\Lambda_\pi = 5.8\mu$ ($\mu = 139.6$ MeV). To get the proper binding energy of the triton taking the Bonn-B potential and the TM 3NF, a value of $\Lambda_\pi = 4.55\mu$ should be used. Such decrease of Λ_π would reduce the effects of the TM 3NF significantly. Therefore the 3NF effects presented in this paper are an overestimation of effects caused by this 3NF model in our breakup configurations.

The data for the low energy Nd elastic scattering vector analyzing power show a drastic discrepancy to theory. Charge independence breaking of the NN interaction in ^3P_J states is a candidate for the explanation of this puzzle [23]. In order to study the ^3P_J sensitivity of breakup analyzing power we performed an additional calculation using the Bonn-B potential with modifications in its ^3P_J force components for the pp and np two-body subsystems as proposed in Ref. [23].

In all calculations performed with $2N$ interactions only we included all $3N$ states with total angular momenta $j \leqslant 3$ of the two-nucleon subsystem. In the case of the calculation with TM 3NF we restricted them to $j \leqslant 2$ due to computer limitations.

III. EXPERIMENT

The measurement presented in this paper was performed at the Cologne FN tandem Van-de Graaff accelerator facility. The polarized protons were produced by a Lamb-shift source as described in [24] and then accelerated to a laboratory energy of 19 MeV. We obtained a typical beam current of 200 nA on target and an average vector polarization $\bar{p_y}$ of 0.8. The beam was focused into an ORTEC 2800 scattering chamber which was modified by a hemispherical 2π extension in order to measure the noncoplanar configuration SST. Behind the scattering chamber the beamline was terminated by a Faraday cup with an integrated (but electrically insulated) ^{4}He gas polarimeter. Four silicon surface barrier detectors, mounted under relative azimuthal angles of $\Delta\Phi = 90°$, allowed continuous monitoring of the transverse beam polarization components p_y and p_x using the known vector analyzing power of the reaction $^4\mathrm{He}(\vec{p},p)$ at $\Theta^{\mathrm{lab}} = 112°$ [25]. The target foils used in our measurement consisted of solid polyethylene $(CD_2)_n$ with a deuterium target thickness of about 80–100 μg/cm^2. In order to extend the lifetime of the foils they were mounted on rotating target holders. This technique reduced the deuterium loss to approximately 1% per hour. The size and shape of the beam spot on target was controlled using a quartz plate with a center hole. The observed beam spot had a typical diameter of 1–2 mm.

For the detection of the outgoing protons of the pd breakup reaction we used cooled ($\approx 0°$C) 2000 μm thick silicon surface barrier detectors with an energy resolution of about 20–40 keV FWHM. The centers of the entrance aperture of the detectors were positioned with an accuracy of $\pm 0.1°$. Table I lists the scattering and solid angles for all coincidence detectors. If we denote by $(\Theta_3, \Theta_4, \Delta\Phi_{34})$ the (laboratory) polar angles and the relative azimuthal angles of the detected breakup protons p_3 and p_4, then the corresponding detector pairs defining the kinematical configura-

TABLE I. Angular parameters (laboratory system). Listed are the detector positions Θ and Φ ($\pm 0.1°$), the angular resolutions in $\Delta\Theta$ and $\Delta\Phi$ direction, the distances to the target r (± 1 mm), and the solid angles $\Delta\Omega$ ($\pm 8\times10^{-3}$ msr).

Θ (deg)	Φ (deg)	$\Delta\Theta$ (deg)	$\Delta\Phi$ (deg)	r (mm)	$\Delta\Omega$ (msr)
41	0	1.0	2.7	231	0.847
52	0	0.7	3.7	231	0.860
52	60	0.9	2.6	244	0.737
63	0	0.7	2.9	260	0.560
41	180	1.0	2.2	230	0.660
52	180	0.7	3.7	230	0.835
52	120	0.9	2.6	247	0.732
63	180	0.7	2.9	260	0.560

tions QFS, FSI, COL, and SST of the present study are characterized by the triplets of angles (41°,41°,180°), (41°,63°,180°), (52°,63°,180°), and (52°,52°,120°), respectively. Note that the configurations FSI, COL, and SST were realized twice. In the case of FSI and COL the second detector arrangement is obtained by a 180° rotation around the beam axis and in the SST case by a corresponding 60° rotation. These symmetric arrangements increased the breakup counting rates by a factor of 2 and helped in reducing the systematic errors of the analyzing powers in the case of FSI and COL (analogously to the two-body case as proposed in [26]). Furthermore, the simultaneous use of one detector in several kinematical configurations increases the possibility to cross-check the consistency of the measurements.

Both detectors at $\Theta^{lab} = 63°$ served simultaneously as monitor detectors and were used for absolute normalization of the breakup cross sections. For the given beam current, the target thickness and the solid angles the total counting rate for each detector was on the order of 5 kHz and therefore significant pile-up effects were not expected. The necessary dead-time corrections were typically in the range of 1–3%.

The signals from all detectors were processed simultaneously by standard fast-slow coincidence electronics and then recorded in list mode on magnetic tape using the Cologne FERA analyzer system [27]. For each coincidence event the stored information consisted of a logical status word (indicating the kinematical configuration), the energies and the time-of-flight differences of the detected particles. A powerful software for online analysis [28,29] was used to check the coincidence events not only by incrementing and displaying two-dimensional energy spectra but also by generating the background-corrected projections of the breakup events onto the relevant kinematical loci.

IV. ANALYSIS OF THE LIST MODE DATA

For a comparison of the experimental results of a kinematically complete three-body breakup measurement with the corresponding theoretical predictions one has to convert the yield of true breakup events into ''S curve'' spectra. The S curve is a one-dimensional representation (arc length) of the kinematically allowed (E_i,E_j) energy values (kinematical curve) of the two detected outgoing nucleons

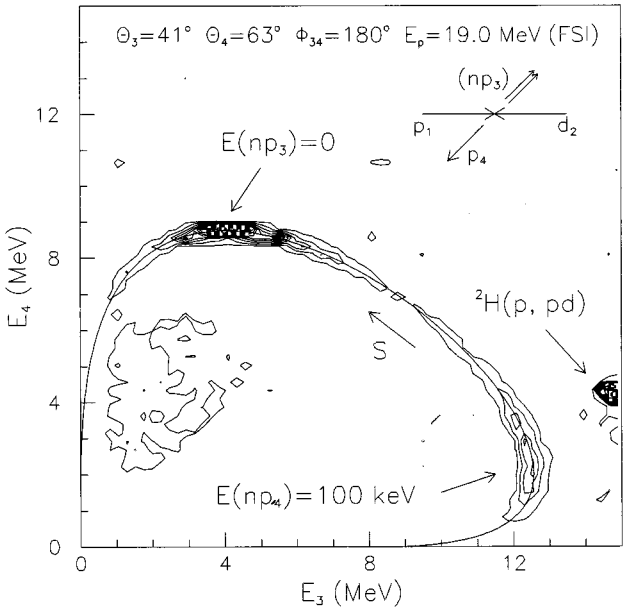

FIG. 1. Calibrated (E_3,E_4) coincidence matrix for the FSI configuration.The positions on the kinematical curve, which correspond to the relative-energy minima $E_{(np_3)}$ and $E_{(np_4)}$ are indicated. Two-body coincidences are visible at $(E_3,E_4)\approx(14.7\text{ MeV},4.2\text{ MeV})$. The remaining low-energy background originates from breakup reactions on the target nuclei ^{12}C.

$i,j=3,4,5$, $i\neq j$ (see, for example [30]). Furthermore, the yield has to be converted to absolute values of the cross sections or, when using polarized projectiles, appropriate ratios of yields have to be taken to get the analyzing powers.

The off-line energy calibration of our coincidence spectra was done using the elastically and inelastically scattered protons and deuterons from the reactions $^{12}C(p,p)^{12}C$, $^{12}C(p,p)^{12}C^{1}*$, $^2H(p,p)^2H$, and $^2H(p,d)^1H$. A linear calibration was essentially sufficient. Figure 1 shows a calibrated and background-corrected (E_3,E_4) matrix for the FSI configuration as a contour plot in arbitrary units. Events closer to the energy axes than to any point on the kinematical curve in the region of interest were not incremented. The calculated point-geometry kinematical curve is also shown. For the projection procedure which assigns the breakup events to the kinematical loci for point geometry, we assumed a simple two-dimensional Gaussian distribution for the (E_3,E_4) pairs. This means that the projection point on the S curve is given directly by the shortest distance between the point-geometry kinematical curve and the (E_3,E_4) event. The assignment of each (E_3,E_4) event to its proper location on the S curve is done by using ''reference matrices.'' For every event in the calibrated (E_3,E_4) plane they contain the numerically calculated information about the shortest distance to the S curve.

The background in our (E_3,E_4) matrices consisted mainly of random coincidences due to elastic and inelastic reactions with the target nuclei ^2H and ^{12}C. The background correction was done using methods similar to those described in [31]. For each event we calculated the ''theoretical'' time-of-flight difference using the known distances of the detectors to the target and the measured energies and assuming the particle masses to be those of the detected nucleons of the pd breakup. ''Time'' matrices were built by sorting the events according to their theoretical time-of-flight

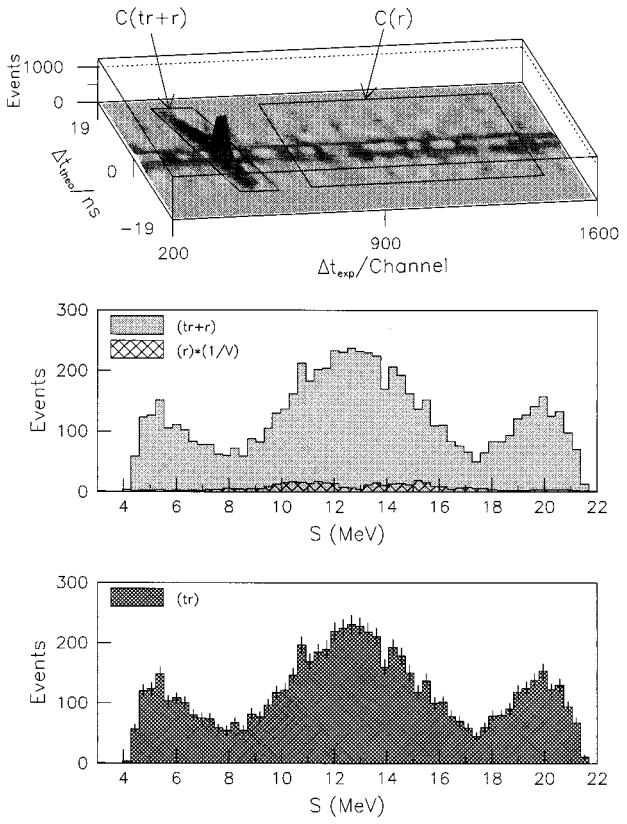

FIG. 2. Background subtraction using time matrices. The theoretical time-of-flight differences are plotted versus the measured time-of-flight differences (top). In the middle part of the figure the resulting S curve spectra of "true+random" and "random" (weighed by a factor $1/V$, see text) cuts are shown. The bottom part of the figure results after background subtraction.

difference and the measured time-of-flight difference (Fig. 2, top). The true pd breakup events which have to show a fixed relation between the theoretical time-of-flight difference and the experimental time-of-flight difference produce a peak above the uniformly distributed random coincidence events. The region marked $C(tr+r)$ containing this peak defines the selection criterion or filter for the true breakup events. This region still contains a contribution from random coincidences which has to be determined. This was done by an interpolation using a filter marked $C(r)$ and containing purely random coincidences (see Fig. 2, top). In order to reduce the statistical errors of the background substraction this region is chosen to be larger by a factor V relative to the experimental time-of-flight difference. After application of our projection procedure to both regions $C(tr+r)$ and $C(r)$ the fraction of true pd breakup events N_{tr} is given by

$$N_{tr}(\Delta S_\mu)=N_{tr+r}(\Delta S_\mu)-\frac{1}{V}N_r(\Delta S_\mu), \tag{4.1}$$

with a statistical error of

$$\Delta_s N_{tr}(\Delta S_\mu)=\sqrt{N_{tr+r}(\Delta S_\mu)+\frac{1}{V^2}N_r(\Delta S_\mu)}. \tag{4.2}$$

ΔS_μ denotes discrete bins on the S curve. In the middle part of Fig. 2 examples for both projected S curve spectra are shown. The bottom part of Fig. 2 displays the resulting spectra.

The normalization of the yield of our S curve spectra was done using the monitor reaction $^2\mathrm{H}(p,p)^2\mathrm{H}$ (see, e.g., [32]). We used a measured cross-section angular distribution at 19 MeV for the pd elastic scattering and interpolated it to our laboratory monitor angle of 63° [33]:

$$\left(\frac{d\sigma}{d\Omega}\right)_M=(28.8\pm0.3)\ \mathrm{mb/sr}. \tag{4.3}$$

Note that our breakup cross-section results could easily be renormalized if a different value of the monitor cross section became available:

$$\left(\frac{d^3\sigma}{d\Omega_3 d\Omega_4 dS}\right)'=\frac{(d\sigma/d\Omega)_{M'}}{(d\sigma/d\Omega)_M}\left(\frac{d^3\sigma}{d\Omega_3 d\Omega_4 dS}\right), \tag{4.4}$$

where $(d\sigma/d\Omega)_{M'}$ denotes the alternative value for the monitor cross section at the corresponding energy and angle. In order to determine the vector analyzing powers as a function of the arc length S we first determined the average value of the beam polarization during the measurement runs. The average value of the beam polarization was $\bar{p}_y=0.795\pm0.012$ for the COL and SST configurations and $\bar{p}_y=0.797\pm0.012$ for the FSI and QFS configurations. These beam polarization values were determined using a ^{4}He polarimeter with the usual Madison convention for the y axis. The spin quantization axis of the polarimeter was parallel to the axis used for the determination of the analyzing powers of the breakup reaction. In the case of the space-star configuration the detector arrangement corresponded to an asymmetric frame for noncoplanar breakup geometries as proposed by Ohlsen *et al.* [34]. In this case the spin quantization axis y is perpendicular to a plane defined by the direction of the momenta of the projectiles ($\vec{p}_1$) and the direction of the momenta of one of the observed particles ($\vec{p}_3$). For each bin ΔS_μ of the kinematical curve we then calculated ratios of breakup events corresponding to the two polarization states "up" and "down" (the two possible directions of the beam polarization vector parallel and antiparallel to the y axis). If $N_1=(N_l^\uparrow N_r^\downarrow)^{1/2}$ and $N_2=(N_l^\downarrow N_r^\uparrow)^{1/2}$ denote the geometric average of the breakup yields N corresponding to the detector arrangements "left" (l) and "right" (r) and polarization states "up" ($\uparrow$) and "down" ($\downarrow$), respectively, then the vector analyzing power in the coplanar configurations FSI and COL was given by

$$A_y(\Delta S_\mu)=\frac{1}{\bar{p}_y}\frac{N_1(\Delta S_\mu)-N_2(\Delta S_\mu)}{N_1(\Delta S_\mu)+N_2(\Delta S_\mu)}. \tag{4.5}$$

In the symmetric coplanar case of pp QFS and the noncoplanar SST case we used an analogous equation but instead of the geometric averages we simply took $N^\uparrow$ and $N^\downarrow$ and normalized the runs for different spin states using the same monitoring reaction as in the case of the cross sections.

The errors of the results of our measurement have different origins. In the case of the cross sections the main sys-

tematic error is due to the normalization factors. The errors of these factors consist of the errors of the normalization cross section and the errors of the solid angles. We determined an overall error for these factors to be about 2%. Another systematic error originates from the projection procedure. Because of the finite angular resolution the breakup events were distributed around the kinematical point-geometry loci. Therefore we had to select a maximum distance from the S curve (''distance cut'') within which the true breakup events were expected. We chose distances of typically 1 MeV. The loss of breakup events corresponding to these cuts was checked by comparing cuts using different values for the maximum distance from the S curve. The loss of true breakup events due to these cuts are estimated to be about 1%. Statistical errors originate from the absolute breakup yield and the background subtraction [Eq. (4.2)]. These errors depend obviously on the chosen bin width ΔS_μ and in our measurement had values in the range of 1–4%. The errors of the analyzing powers were calculated using the errors of the average beam polarizations and the statistical errors as given by Eq. (4.2). In the case of the QFS and SST configurations the normalization of the runs for the different spin states required normalization factors on the order of 1.01 with negligible errors.

V. RESULTS AND DISCUSSION

In Figs. 3–6 we present the experimental results for cross sections and analyzing powers in all four kinematical configurations studied. The data are presented as a function of the arc length of the S curve plotted counterclockwise with zero chosen at the intersection of the kinematical curve with the E_3 axis.

The cross-section data for FSI and COL configurations (Figs. 3 and 4, respectively) show good agreement in large parts of the S curve with the point-geometry predictions of all NN potentials used. We show in Figs. 3 and 4 only the predictions of Bonn-B and Nijm I but the theoretical cross sections for both configurations are very stable when one NN potential is replaced by another. Discrepancies are visible only in the regions of an exact FSI condition or close to it, which correspond to minima of the relative energy of an np pair. For the FSI configuration they result from finite angular resolutions of the experimental setup and the chosen bin width ΔS_μ. Taking, namely, into account the finite geometry of the two proton detectors and performing a suitable averaging of the theoretical point-geometry predictions over solid angles of both detectors leads to a drastic improvement of the agreement between data and theory for this configuration. A similar behavior was found in our previous study at 13 MeV [5] and shows how important it is in some pd breakup configurations to account exactly for the experimental conditions before a comparison between theory and data is performed—especially if one wants to extract the a_{np} scattering length from the np FSI peak. The inclusion of the TM 3NF leads to changes of the FSI cross section of about 10% relative to the results of the pure $2N$ calculation. The largest effects are seen in the region of the FSI peak where this 3NF increases the cross section thereby moving the theory away from the data. For the collinear configuration the effects are mostly negligible except for the region near the FSI condition. The region around the collinear point ($S \approx 11.5$ MeV in Fig. 4) seems to be insensitive to changes induced by the inclusion of the TM 3NF, contrary to expectations based on simple model predictions [35].

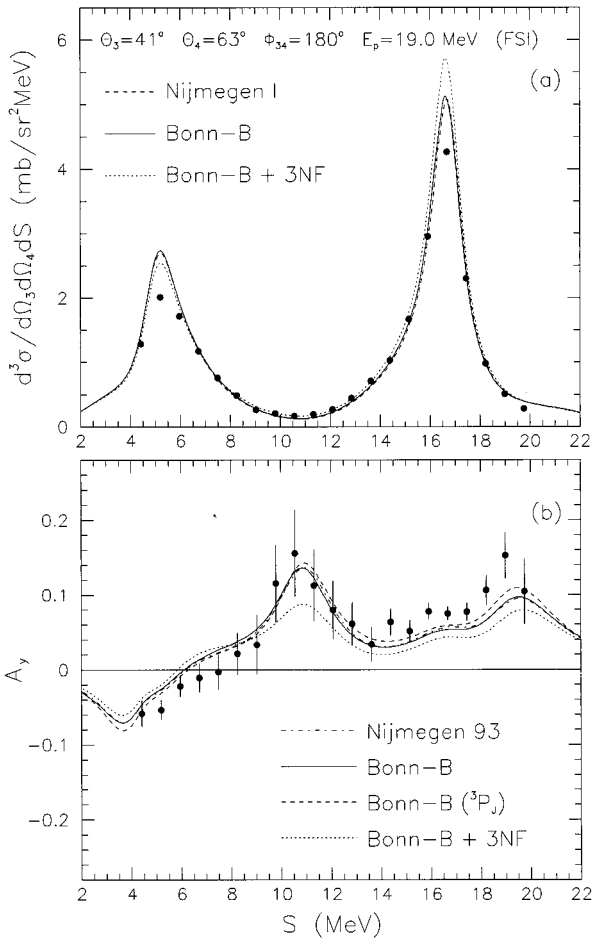

FIG. 3. The breakup cross sections (a) and analyzing powers (b) for the FSI configuration. The experimental data (solid dots) are compared with the results of Faddeev calculations using the Bonn-B, Nijmegen I, and Nijmegen 93 potentials. Also results of Bonn-B + TM 3NF calculations are shown. In the case of the breakup cross sections the statistical errors are smaller then the solid dots' size. For A_y the dashed line denoted by Bonn-B (^3P_J) results when Bonn-B ^3P_J NN force components are modified for pp and np systems according to the prescription of [23].

The analyzing power is reproduced reasonably well in both configurations by the theoretical predictions based on $2N$ forces only. For A_y, however, in contrast to the cross section, the changes resulting from inclusion of the TM 3NF are dramatic (up to about 50% depending on the region of S curve) and nearly everywhere they take theory away from the data. One should, however, emphasize that these TM 3NF effects correspond to $\Lambda_\pi = 5.8\mu$. Taking $\Lambda_\pi = 4.55\mu$ corresponding to a situation where this TM 3NF together with the Bonn-B potential reproduces the triton binding energy would reduce the resulting effects drastically [2,3] such that they would be practically negligible both for cross sections and analyzing powers in all four breakup configurations studied here.

The experimental data for the SST configuration are shown in Fig. 5. The theoretical cross sections overestimate

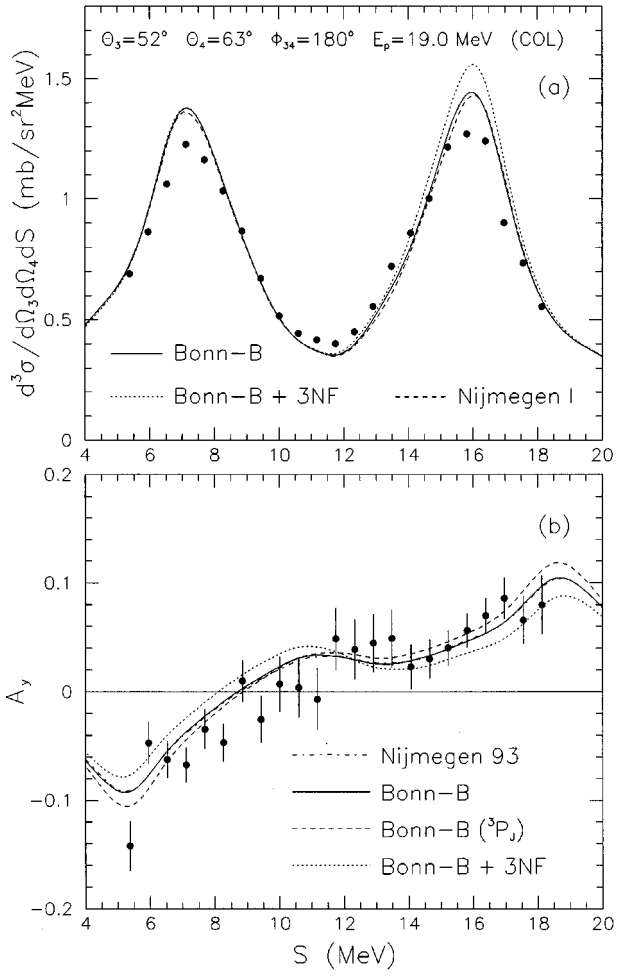

FIG. 4. The same as Fig. 3 but for the COL configuration.

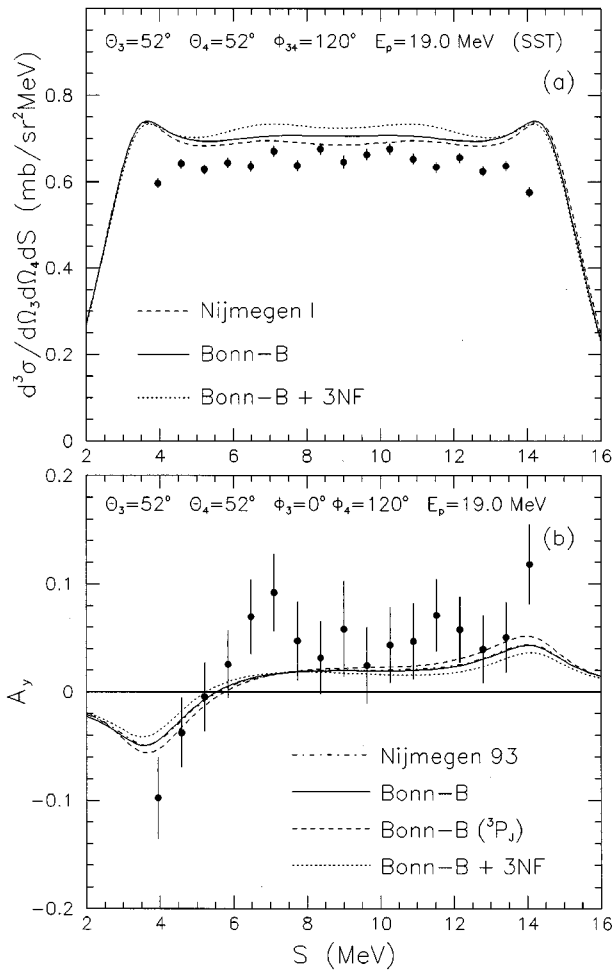

FIG. 5. The same as Fig. 3 but for the SST configuration.

our pd data by about 7%. A similar behavior of this specific configuration was seen at 10.5 [36] and 13 MeV [5] with theory overshooting the data by about 20%. On the other side the nd measurements for this configuration performed at 10.3 [4,37] and 13 MeV [38] delivered nd data laying clearly above the corresponding pd data. One set of 10.3 MeV nd data [4] is in quite good agreement with the theoretical predictions, another one [37] lying however clearly above the theory by about 20% [3]. These two sets of nd data are thus in contradiction to one another. At 13 MeV nd data of Ref. [38] disagree with pure $2N$ potential predictions [7] which underestimate the SST cross-section data by about 20%. Recent independent measurements performed at TUNL [39] support the SST results of Ref. [38]. Taking into account TM 3NF lowers the space-star cross section at 10.5 and 13 MeV relative to the pure $2N$ force prediction, moving the theory away from the nd data and closer to the pd data. As can be seen in Fig. 5, however, at 19 MeV the TM 3NF acts opposite, increasing the SST cross section slightly by about 3%, taking the theory away from our pd data. The smallness of the TM 3NF effects on the SST cross section together with strongly reduced disagreement between our pure $2N$ force predictions and present pd data as compared to the corresponding larger disagreement at 10.5 and 13 MeV suggests that it originates probably from Coulomb force acting between two protons which is totally neglected in the theory. The very good agreement between our theory and recent pd cross section data for the space star at 65 MeV [10] gives additional support for such a conclusion. However, it should be stressed, that only $3N$ breakup calculations which include the pp Coulomb force exactly could help solve unambiguously the problem of the disagreement existing for pd data. The first step in this direction performed recently indicates quite large effects (up to 20%) of the Coulomb force on the breakup cross sections [40]. Unfortunately, the NN force used was a rank-one separable Yamaguchi force and the question remains whether the effects will also be present for realistic forces and higher partial waves taken into account. Similar as for the FSI and COL configurations cross sections for the SST configuration are stable against interchanging NN forces.

The comparison of the analyzing-power data with the theoretical predictions shows that—although the error bars are quite large and the value of A_y rather small—the shape and magnitude are reproduced reasonably by the theory. Here the changes induced by the TM 3NF are smaller then in FSI and COL configurations and—as there—tend away from the A_y data.

In the QFS configuration presented in Fig. 6 we found a very large discrepancy between the theoretical cross section and our pd data. A comparison with the corresponding pd data at 10.5 [36] and 13 MeV [5] reveals that there the dis-

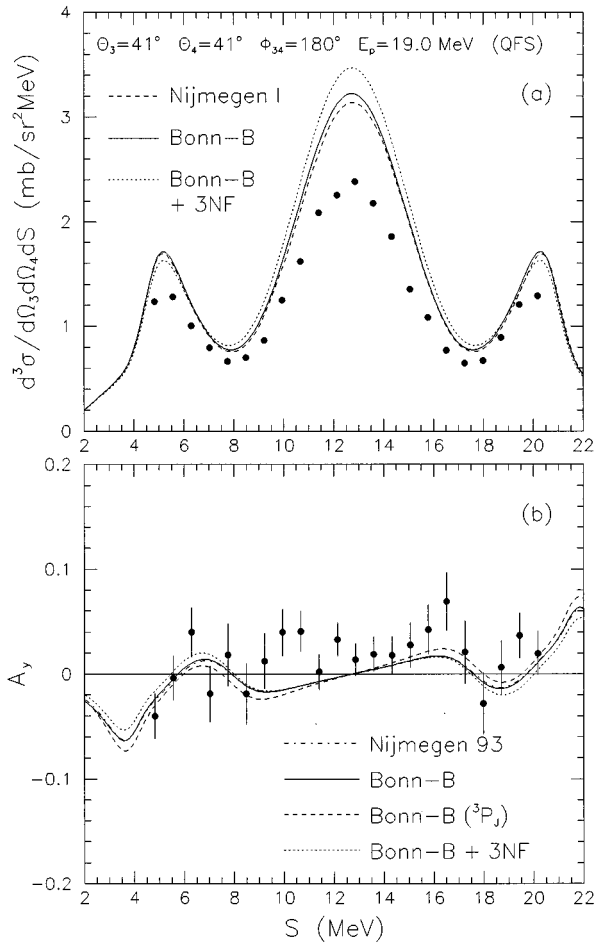

FIG. 6. The same as Fig. 3 but for the QFS configuration.

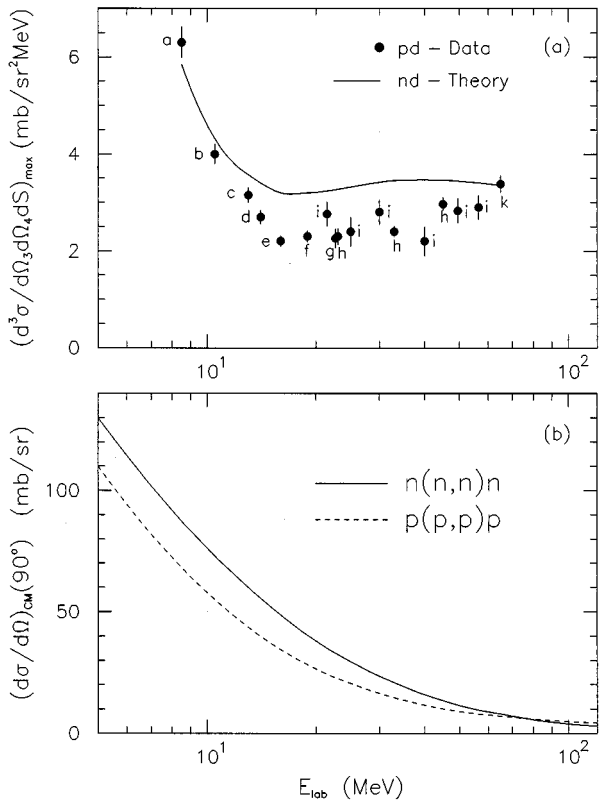

FIG. 7. Part (a) shows published cross-section data (solid dots) under the pp QFS condition together with the corresponding nd Faddeev calculations using the Bonn-B potential. The corresponding references from which data were taken are a: [44], b: [36], c: [5], d: [43], e: [32], f: this paper, g: [8], h: [41], i: [42], k: [45]. Part (b) shows cross sections for free pp and nn scattering calculated with Bonn-B potential.

crepancies were mainly restricted to the region of QFS peak while at 19 MeV they exist practically along the entire S curve. The inclusion of the TM 3NF even increases these discrepancies. For the QFS analyzing power definite conclusions cannot be drawn due to the large experimental errors and large scatter of data. QFS cross sections are also stable against interchanges of NN interactions with the exception of the region at and close to QFS condition where small differences between different potentials are visible. They reflect different properties of their $^3S_1-{}^3D_1$ force components.

In order to gain some insight into the systematics of the deviations found in the QFS configuration we compared some published QFS peak cross-section data in the incoming proton laboratory energy range from 8.5 to 65 MeV with corresponding theoretical predictions obtained with the Bonn-B potential. In Fig. 7 (a) we show our most recent pp QFS data together with the older ones, also obtained at our laboratory, and data of other groups. For this purpose we adjusted some of the older data. The data points at 8.5, 14.1, and 16.0 MeV were renormalized using Eq. (4.4) and more recent elastic cross-section pd data of Ref. [33]. The resulting modifications are of the order of 4%. For some of the data points above 20 MeV which were given originally in the form of projections onto one energy axis we changed the corresponding cross section by multiplying it by a factor $1/\sqrt{2}$ to get it projected on the kinematical locus. Finally we point out that most of the data points (especially those of Ref. [42]) were obtained by averaging over 2–4 channels of the original spectra together with new estimates of the corresponding statistical errors. The comparison to theory reveals a clear systematic effect. The discrepancies found are relatively small at energies around 10 and 70 MeV but reach a maximum in the energy range 15–40 MeV. An additional comparison of the calculated cross sections for free pp and nn scattering at $\Theta^{\text{c.m.}}=90°$ [Fig. 7 (b)] which come closely together around 70 MeV, further supports the conclusion that at our energy Coulomb-force effects are probably responsible for the disagreement between 3N theory and QFS pd cross-section data. The nonmonotonic energy dependence of the QFS cross-section discrepancies shows that only full-fledged breakup calculations with pp Coulomb force included exactly could unambiguously determine the magnitude of Coulomb force effects in every individual case.

The analyzing power in low energy Nd elastic scattering presents an unsurmountable problem for all present-day realistic NN interactions [3]. In [23] the solution to this problem was proposed introducing a significant CIB in ^3P_J NN force components on which the elastic-scattering A_y depends in a very sensitive way. As can be seen from Figs. 3–6 also breakup analyzing powers in our configurations are sensitive to such changes of ^3P_J NN force components. Generally speaking, practically in all cases the changes of A_y thus in-

TABLE II. Reduced χ^2 of the analyzing powers for different potentials. TM denotes "Bonn-B + TM 3NF."

	N	AV14	Nijm78	Paris	Bonn-B	mod. Bonn-B	TM
FSI	21	2.7	1.3	1.9	1.9	1.1	3.7
COL	23	1.8	1.1	1.3	1.3	1.1	2.2
QFS	22	1.8	1.6	1.7	1.6	1.6	1.8
SST	17	1.3	1.2	1.2	1.2	1.0	1.4

	N	AV18	CD Bonn	Nijm93	NijmI	NijmII
FSI	21	1.7	1.8	1.7	1.5	1.6
COL	23	1.2	1.2	1.2	1.1	1.1
QFS	22	1.6	1.6	1.6	1.6	1.6
SST	17	1.2	1.1	1.2	1.1	1.2

duced are non-negligible and bring theory closer to the data.

In order to give a quantitative comparison of the theoretical predictions for the analyzing powers we calculated a reduced χ^2 for all potentials used:

$$\chi^2/N=\frac{1}{N}\sum_{i=1}^{N}\frac{[A_{y,i}^{\mathrm{theo}}(S)-A_{y,i}^{\mathrm{exp}}(S)]^2}{[\Delta A_{y,i}^{\mathrm{exp}}(S)]^2}. \tag{5.1}$$

The results are given in Table II. From this table we see that (i) the calculation using the ${}^3P_J$ *pp-np* modified Bonn-B potential shows the smallest reduced χ^2 in nearly all cases; (ii) the inclusion of the TM-3NF increases the disagreement between measured and calculated analyzing powers; (iii) all predictions with different potentials, with the exception of AV14, do not differ substantially; (iv) AV14 predictions show always the largest χ^2 which reflects its quite different ${}^3P_J$ forces as compared to other potentials [3].

VI. SUMMARY

We present new cross-section and vector analyzing-power data in four kinematically complete configurations of the *pd* breakup reaction at 19.0 MeV. The data are compared to predictions of rigorous three-nucleon Faddeev calculations using different realistic nucleon-nucleon potentials. The resulting picture for the cross sections is found to be stable against replacing one *NN* force by another, with the exception of the QFS configuration which reflects differences in the ${}^3S_1-{}^3D_1$ force component of some potentials used. For the cross sections discrepancies between theory and data are found for SST and, especially large, for the QFS, whereas a good agreement exists in the case of the FSI and COL configurations. The systematics of QFS and SST results at different energies can be interpreted as a signature of strong Coulomb-force effects in the *pd* system for these specific configurations at our energy. The inclusion of the Tucson-Melbourne three-nucleon potential in practically all cases moves the theory away from experimental data both for cross sections and analyzing powers. The vector analyzing powers for the FSI and COL configurations are described slightly better when using a version of the Bonn-B potential which was phenomenologically modified by introducing CIB in the ${}^3P_J$ force components.

ACKNOWLEDGMENTS

This work was supported financially by the Deutsche Forschungsgemeinschaft (Project Nos. Pa 488/1-1 and Pa 488/1-2), by the Bundesministerium für Forschung und Technologie [Project No. 06 BO 738(7)], and by the Polish Committee for Scientific Research under Grant No. 2 P302 104 06. The numerical calculations were performed on the CRAY Y-MP of the Höchstleistungsrechenzentrum in Jülich, Germany.

[1] H. Witała, Th. Cornelius, and W. Glöckle, Few-Body Syst. **3**, 123 (1988).
[2] D. Hüber, H. Witała, and W. Glöckle, Few-Body Syst. **14**, 171 (1993).
[3] W. Glöckle, H. Witała, H. Kamada, D. Hüber, and J. Golak, in *Few-Body Problem in Physics*, AIP Conf. Proc. 334, Williamsburg, Virginia, 1994, edited by F. Gross (AIP, New York, 1995), p. 45.
[4] M. Stephan, K. Bodek, J. Krug, W. Lübcke, S. Obermanns, H. Rühl, M. Steinke, D. Kamke, H. Witała, Th. Cornelius, and W. Glöckle, Phys. Rev. C **39**, 2133 (1989).
[5] G. Rauprich, S. Lemaître, P. Nießen, K. R. Nyga, R. Reckenfelderbäumer, L. Sydow, H. Paetz gen. Schieck, H. Witała, and W. Glöckle, Nucl. Phys. **A535**, 313 (1991).
[6] M. Allet, K. Bodek, W. Hajdas, J. Lang, R. Müller, O. Naviliat-Cuncic, J. Sromicki, J. Zejma, L. Jarczyk, St. Kistryn, J. Smyrski, A. Strzałkowski, W. Glöckle, J. Golak, H. Witała, B. Dechant, J. Krug, and P. A. Schmelzbach, Phys. Rev. C **50**, 602 (1994).
[7] H. Witała, Th. Cornelius, and W. Glöckle, Few-Body Syst. **5**, 89 (1988).
[8] M. Zadro, M. Bogovac, G. Calvi, M. Lattuada, D. Miljanić, D. Rendić, C. Spitaleri, B. Vlahović, H. Witała, W. Glöckle, J. Golak, and H. Kamada, Nuovo Cimento **107**, 185 (1994).
[9] M. Allet, K. Bodek, W. Hajdas, J. Lang, R. Müller, S. Navert, O. Naviliat-Cuncic, J. Sromicki, J. Zejma, L. Jarczyk, St. Kistryn, J. Smyrski, A. Strzałkowski, H. Witała, W. Glöckle, J. Golak, D. Hüber, and H. Kamada, Few-Body Syst. (to be published).
[10] J. Zejma, Ph.D. thesis, Jagellonian University, Cracow, 1995, (unpublished).
[11] H. Witała, D. Hüber, and W. Glöckle, Phys. Rev. C **49**, R14 (1994).
[12] W. Glöckle, *The Quantum Mechanical Few-Body Problem* (Springer-Verlag, Berlin, 1983).
[13] H. Witała, W. Glöckle, and H. Kamada, Phys. Rev. C **43**, 1619 (1991).
[14] R. B. Wiringa, R. A. Smith, and T. L. Ainsworth, Phys. Rev. C **29**, 1207 (1984).
[15] R. Machleidt, Adv. Nucl. Phys. **19**, 189 (1989).
[16] M. M. Nagels, T. A. Rijken, and J. J. de Swart, Phys. Rev. D **17**, 768 (1978).
[17] M. Lacombe, B. Loiseau, J. M. Richard, R. Vinh Mau, J. Côté , P. Pirès, and R. de Tourreil, Phys. Rev. C **21**, 861 (1980).

[18] R. B. Wiringa, V. G. J. Stoks, and R. Schiavilla, Phys. Rev. C **51**, 38 (1995).
[19] R. Machleidt (private communication).
[20] V. G. J. Stoks, R. A. M. Klomp, C. P. F. Terheggen, and J. J. de Swart, Phys. Rev. C **49**, 2950 (1994).
[21] S. A. Coon, M. D. Scadron, P. C. McNamee, B. R. Barrett, D. W. E. Blatt, and B. H. J. McKellar, Nucl. Phys. **A317**, 242 (1979).
[22] S. A. Coon and W. Glöckle, Phys. Rev. C **23**, 1790 (1981).
[23] H. Witała and W. Glöckle, Nucl. Phys. **A 528**, 48 (1991).
[24] V. Bechtold, L. Friedrich, P. Ziegler, R. Aniol, G. Latzel, and H. Paetz gen. Schieck, Nucl. Instrum. Methods **150**, 407 (1978).
[25] L. Sydow, S. Vohl, S. Lemaitre, P. Nießen, K. R. Nyga, R. Reckenfelderbäumer, G. Rauprich, and H. Paetz gen. Schieck, Nucl. Instrum. Methods Phys. Res. Sect. A **327**, 441 (1993).
[26] G. G. Ohlsen and P. W. Keaton, Nucl. Instrum. Methods **109**, 41 (1973).
[27] N. Nicolay, M. Luig, F. Giesen, S. Albers and R. Wirowski, Verhandlungen der Deutschen Physikalischen Gesellschaft (VI) 27, 153 (1992).
[28] R. Großmann, diploma thesis, University of Cologne, 1993.
[29] PAW, CERN Program Library entry **Q121**, ed.: M. Goossens, Genf 1989.
[30] G. G. Ohlsen, Nucl. Instrum. Methods **37**, 240 (1965).
[31] D. Gola, W. Bretfeld, W. Burgmer, H. Eichner, Ch. Heinrich, H. J. Helten, H. Kretzer, K. Prescher, H. Oswald, W. Schnorrenberg, and H. Paetz gen. Schieck, Phys. Rev. C **27**, 1394 (1983).
[32] H. Klein, H. Eichner, H. J. Helten, H. Kretzer, K. Prescher, H. Stehle, and W. W. Wohlfarth, Nucl. Phys. **A199**, 169 (1973).
[33] W. Grüebler, V. König, P. A. Schmelzbach, F. Sperisen, B. Jenny, R. E. White, F. Seiler, and H. W. Roser, Nucl. Phys. **A398**, 445 (1983).
[34] G. G. Ohlsen, R. E. Brown, F. D. Correll, and R. A. Hardekopf, Nucl. Instrum. Methods **179**, 283 (1981).
[35] W. Meier and W. Glöckle, Phys. Lett. **138B**, 329 (1984).
[36] R. Großmann, W. Glöckle, J. Golak, G. Nitzsche, H. Patberg, L. Sydow, S. Vohl, H. Witała, and H. Paetz gen. Schieck, in 14th International IUPAP Conference on Few Body Problems in Physics, Contributed Papers, Williamsburg, 1994; R. Groβmann, G. Nitzsche, H. Patberg, L. Sydow, S. Vohl, H. Paetz gen. Schieck, J. Golak, H. Witała, W. Glöckle, and D. Hüber, Nucl. Phys. A (to be published).
[37] K. Gebhardt, W. Jaeger, C. Jeitner, M. Vitz, E. Finckh, T. N. Frank, Th. Januschke, W. Sandhas, and H. Haberzettl, Nucl. Phys. **A 561**, 232 (1993).
[38] J. Strate, K. Geissdörfer, R. Lin, W. Bielmeier, J. Cub, A. Ebneth, E. Finckh, H. Friess, G. Fuchs, K. Gebhardt, and S. Schindler, Nucl. Phys. **A 501**, 51 (1989).
[39] W. Tornow (private communication).
[40] E. O. Alt and M. Rauh, Few-Body Syst. **17**, 121 (1994).
[41] D. J. Margaziotis, G. Paić, J. C. Young, J. W. Verba, W. J. Braithwaite, J. M. Cameron, D. W. Storm, and T. A. Cahill, Phys. Rev. C **2**, 2050 (1970).
[42] J. L. Durand, J. Arvieux, A. Fiore, C. Perrin, and M. Durand, Phys. Rev. C **6**, 393 (1972).
[43] H. J. Helten, Ph.D. thesis, University of Cologne, 1980.
[44] B. Kühn, H. Kumpf, J. Mösner, W. Neubert, and G. Schmidt, Nucl. Phys. **A247**, 21 (1975).
[45] M. Allet, K. Bodek, W. Hajdas, L. Jarczyk, St. Kistryn, J. Lang, R. Müller, S. Navert, O. Naviliat-Cuncic, J. Smyrski, J. Sromicki, A. Strzałkowski, and J. Zejma, Helv. Phys. Acta **66**, 437 (1993).